Supplemental Materials

Molecular Biology of the Cell

Gerhold et al.

Figure S1

A

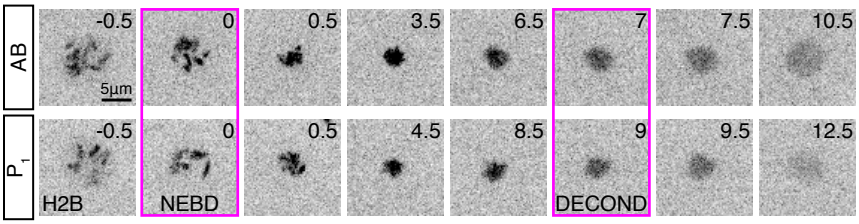
AB
P1
-0.5
0
0.5
3.5
6.5
7
7.5
10.5
4.5
8.5
9
9.5
12.5
5µm
H2B
NEBD
DECOND

B

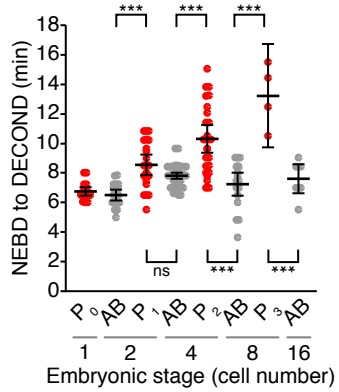
NEBD to DECOND (min)
Embryonic stage (cell number)
***
ns
P0
AB
P1
P2
P3
1
2
4
8
16

Figure S1. Germline P lineage cells show prolonged mitotic delays relative to somatic AB lineage cells when spindle formation is perturbed using a temperature sensitive allele of β-tubulin. Related to Figure 1. (A) Representative cropped time points from an AB (top) and P_1 (bottom) cell carrying *tbb-2(or362)* and H2B::mCH and shifted to the restrictive temperature (26°C), showing the timing of nuclear envelop breakdown (NEBD) to the start of chromosome decondensation (DECOND). Scale bar = 5μm. (B) The duration of mitosis in germline P and somatic AB lineage cells from 1 to 16-cell stage embryos with *tbb-2(or362)*-induced spindle perturbations. Germline P lineage cells (red) delay in mitosis for longer than somatic AB cells at the same and later embryonic stages. Black bars represent the mean. Error bars show the 95% confidence interval for the mean. p values were determined by an Anova1 with Tukey-Kramer post-hoc test, ns = $p > 0.05$, *** = $p < 0.001$. See Table S2 for summary statistics.

Figure S2

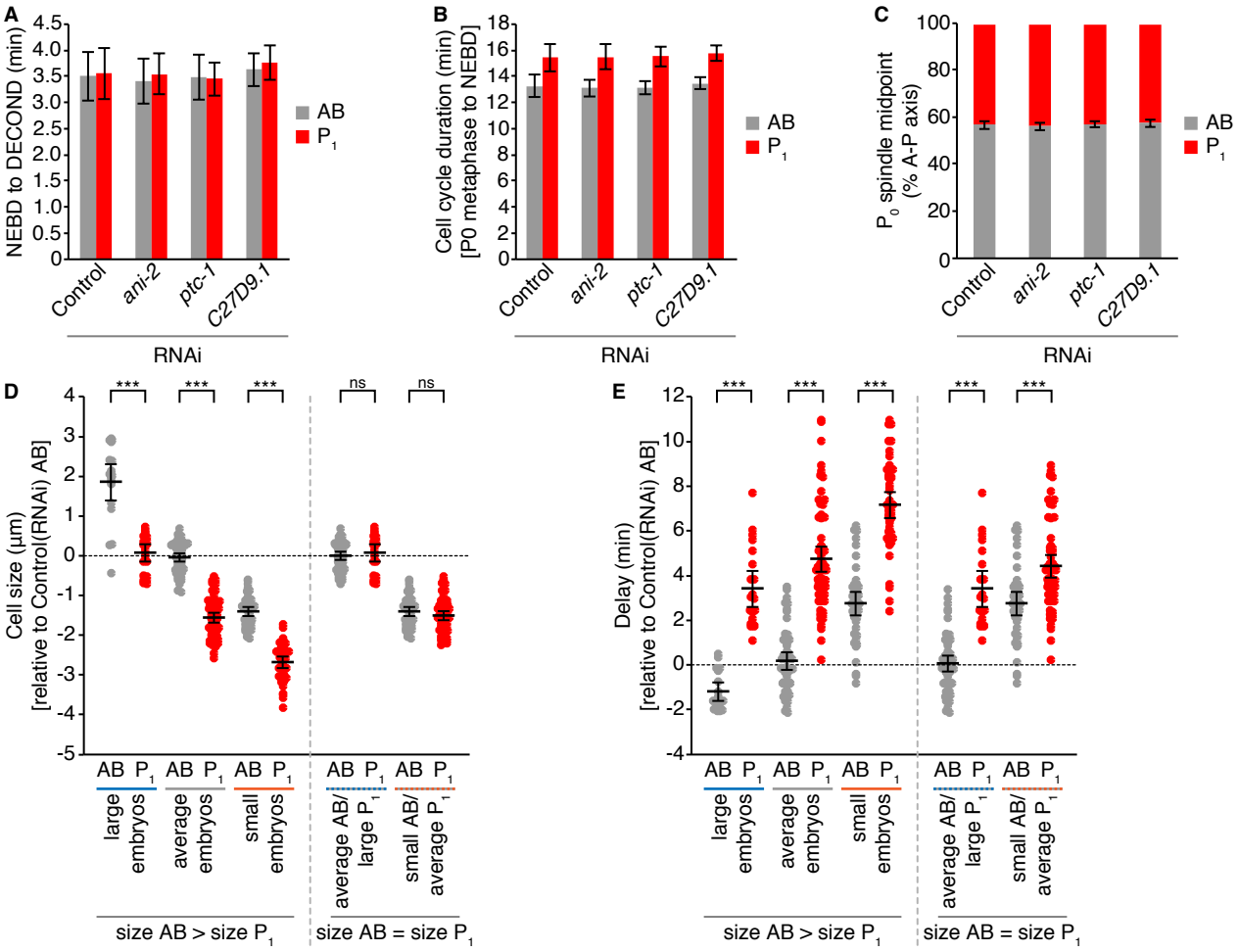
A
NEBD to DECOND (min)
AB
P1
Control
ani-2
ptc-1
C27D9.1
RNAi
B
Cell cycle duration (min)
[P0 metaphase to NEBD]
C
P0 spindle midpoint
(% A-P axis)
D
Cell size (µm)
[relative to Control(RNAi) AB]
***
ns
large embryos
average embryos
small embryos
average AB/ large P1
small AB/ average P1
size AB > size P1
size AB = size P1
E
Delay (min)
[relative to Control(RNAi) AB]

Figure S2. Genetic manipulations to vary embryo size do not affect the timing of bipolar divisions, cell cycle asynchrony between AB and P_1 or spindle positioning in P_0 and can be used to compare the duration of monopolar mitoses in comparably-sized AB and P_1 cells. Related to Figure 4. (A and B) Bar graphs showing the mean duration of bipolar mitoses (A) and cell cycle (B) in AB (grey) and P_1 (red) cells following RNAi-induced changes in embryo volume. Error bars represent ± 1 standard deviation of the mean. (C) Stacked bar graph showing the relative size of AB (grey) and P_1 (red) as inferred from the position of the spindle midpoint in P_0 along the anterior to posterior axis of the embryo. Error bars represent ± 1 standard deviation of the mean. (D-E) Beeswarm plots showing the measurement data, cell size (D) and delay (E), used in the bootstrap analysis presented in Figure 4, C and D. Black bars represent the mean and error bars show the 95% confidence interval. Data were compared using a 2-sample, 2-tailed t-test. ns = $p > 0.05$, *** = $p < 0.001$. See Table S2 for summary statistics.

Figure S3

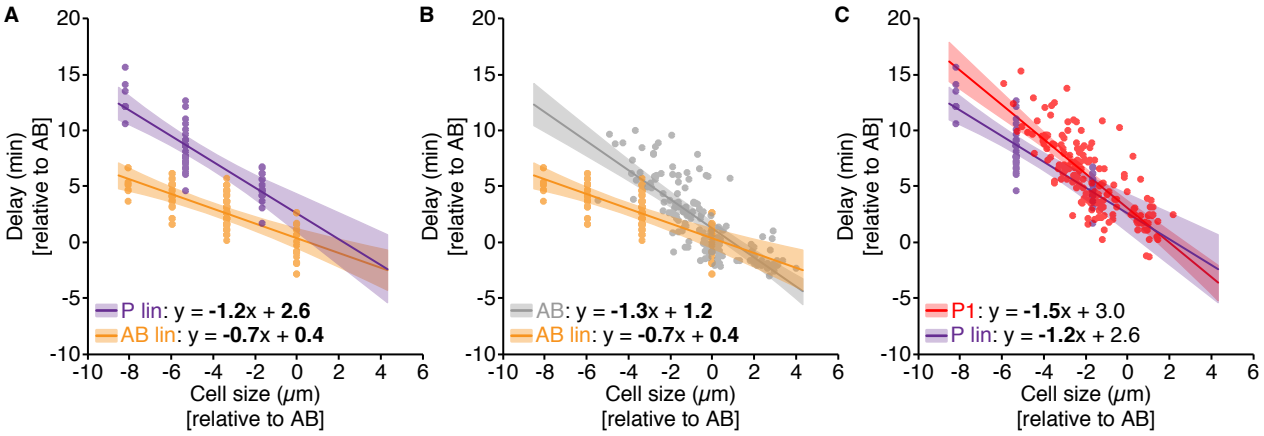
A
B
C
Delay (min)
[relative to AB]
Cell size (μm)
[relative to AB]
P lin: y = -1.2x + 2.6
AB lin: y = -0.7x + 0.4
AB: y = -1.3x + 1.2
AB lin: y = -0.7x + 0.4
P1: y = -1.5x + 3.0
P lin: y = -1.2x + 2.6

Figure S3. Genetically reducing embryo volume produces longer mitotic delays than comparable developmental reductions in cell size**.** Related to Figures 2 and 4. (A) The duration of monopolar mitoses (delay) in cells from the germline P lineage (red, n = 57, r = -0.85, p = $7.2x10^{-17}$) and somatic AB lineage (grey n = 131, r = -0.74, p = $1.6x10^{-23}$) in 2- to 16-cell embryos relative to mean cell size. All values are expressed relative to (+/-) the mean value for all AB cells at the 2-cell stage. Mean cell size was calculated as in Figure 4, B. Data are independent from that presented in Figure 2, C. The rate at which delay increases with decreasing cell size is greater in the germline P lineage than in the somatic AB lineage. Statistically different regression coefficients are written in bold and were compared using a non-parametric bootstrap (p = 0.013 for slope and p = 0.002 for intercept). (B-C) The duration of monopolar mitoses (delay) relative to cell size for AB (B) or P_1 (C) cells from 2-cell stage embryos in which embryo size was manipulated by RNAi depletion of ANI-2, PTC-1 and C27D9.1 compared to the same relationship for cells within their respective lineages. Data for cells from the AB and P lineages are reproduced from Figure S3, F. Data for AB and P_1 from small/large 2-cell stage embryos are reproduced from Figure 4, B. Genetic manipulation of embryo volume tends to produce longer mitotic delays than similar cleavage-driven reductions in cell size. Regression coefficients were compared using a non-parametric bootstrap, with significant differences written in bold. p = 0 (slope) and p = $5.7x10^{-4}$ (intercept) for AB 2-cell versus AB lineage. p = 0.004 (slope) and p = 0.351 (intercept) for P_1 2-cell versus P lineage. For all panels, lines represent the linear least squares regression fit with 95% confidence interval (shaded regions).

Figure S4

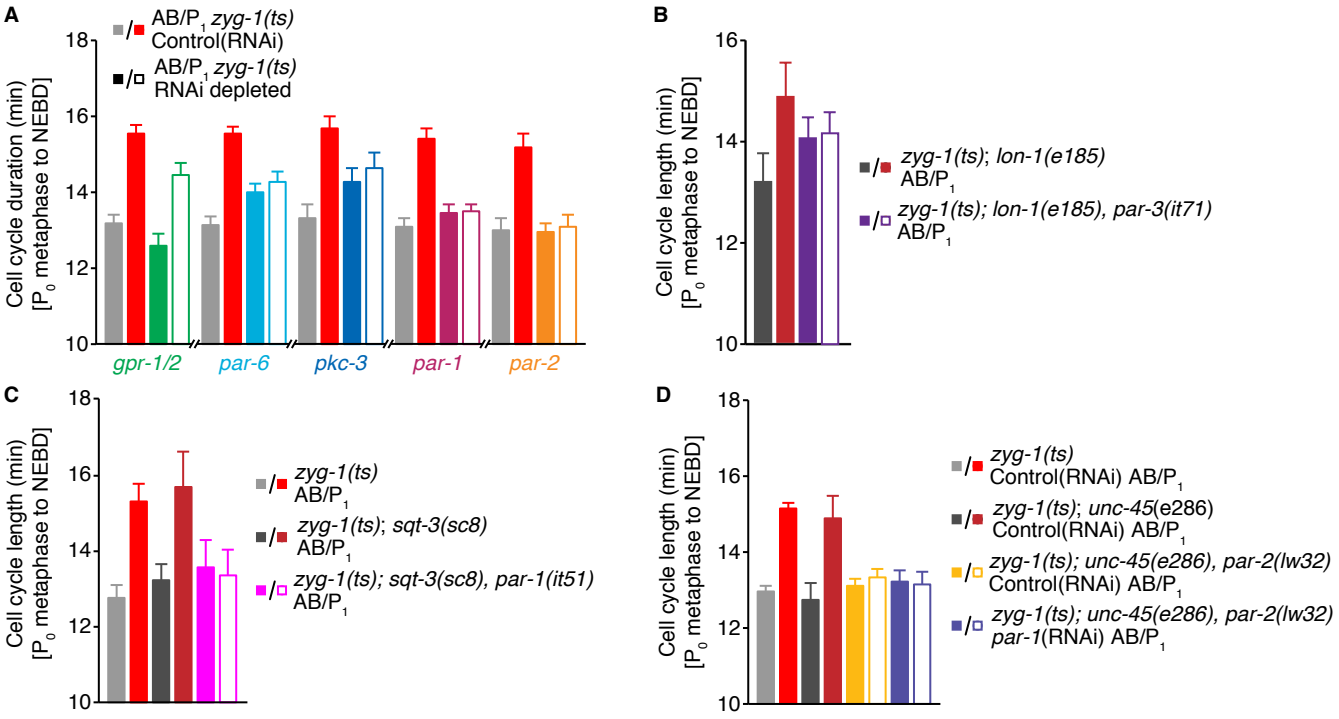
A
Cell cycle duration (min) [P0 metaphase to NEBD]
AB/P1 zyg-1(ts) Control(RNAi)
AB/P1 zyg-1(ts) RNAi depleted
gpr-1/2
par-6
pkc-3
par-1
par-2
B
Cell cycle length (min) [P0 metaphase to NEBD]
zyg-1(ts); lon-1(e185) AB/P1
zyg-1(ts); lon-1(e185), par-3(it71) AB/P1
C
Cell cycle length (min) [P0 metaphase to NEBD]
zyg-1(ts) AB/P1
zyg-1(ts); sqt-3(sc8) AB/P1
zyg-1(ts); sqt-3(sc8), par-1(it51) AB/P1
D
Cell cycle length (min) [P0 metaphase to NEBD]
zyg-1(ts) Control(RNAi) AB/P1
zyg-1(ts); unc-45(e286) Control(RNAi) AB/P1
zyg-1(ts); unc-45(e286), par-2(lw32) Control(RNAi) AB/P1
zyg-1(ts); unc-45(e286), par-2(lw32) par-1(RNAi) AB/P1

Figure S4. AB and P_1 cell cycle durations following RNAi depletion of GPR-1/2 and PAR proteins and in *par-3(it71)*, *par-1(it51)* and *par-2(lw32)* mutants. Related to Figure 5. (A) Cell cycle asynchrony is lost in *par* embryos, with depletion of the posterior PAR proteins, PAR-1 and PAR-2, showing a clear acceleration of cell cycle progression and an AB-like cell cycle duration in P_1. In our hands, loss of anterior PARs tended to produce an intermediate phenotype, with respect to cell cycle duration, rather than an unambiguous P_1-like cell cycle duration in both cells. (B) Cell cycle duration for *par-3(it71)* AB and P_1 cells, with their respective controls. Cell cycle asynchrony is lost, and cell cycle duration in *par-3(it71)* AB and P_1 cells is intermediate to that found in control AB and P_1 cells. (C) Cell cycle duration for *par-1(it51)* AB and P_1 cells, with their respective controls. (D) Cell cycle duration for *par-2(lw32)* AB and P_1 cells, with their respective controls. *par-2(lw32)* P_1, *par-2(lw32), par-1*(RNAi) P_1 and *par-1(it51)* P_1 cells all have accelerated cell cycle durations that resemble control AB cells. For all panels, bar graphs show mean cell cycle length (from metaphase of P_0 to nuclear envelope breakdown of AB or P_1), with filled bars for AB and open bars for P_1 values. Control AB and P_1 values are shown in grey and red, respectively. Error bars show the 95% confidence interval for the mean.

Table S1. *C. elegans* strains used in this study. Related to all figures. All strains, except UM399 (30), were constructed as part of this study using the following: EU782 (*zyg-1(or297) II*), EU858 (*tbb-2(or362) III*), TH27 (*unc-119(ed3) III; ddIs6 [tbg-1::GFP, unc-119(+)] V*), UM397 (*mdf-2(tm2190), ltIs37[unc-119(+), Ppie-1::mCherry::his-58] IV*), LP271 (*cpIs42[mex-5p::mNeonGreen::PLCδ-PH::tbb-2 3'UTR + unc-119(+)]* II; unc-119(ed3) III), UM226 (*ltIs37[unc-119(+), Ppie-1::mCherry::his-58] IV*), KK747 (*unc-45(e286), par-2(lw32)/qC1[dpy-19(e1259), glp-1(q339)] III*), KK292 (*sqt-3(sc8), par-1(it51) V/nT1[unc-?(n754) let-?] (IV;V)*), BC8 (*sqt-3(sc8) V*), CB286 (*unc-45(e286) III*), and KK571 (*lon-1(e185), par-3(it71)/qC1 [dpy-19(e1259) glp-1(q339)] III*). LP271 was kindly provided by Drs. D. Dickinson and B. Goldstein. The *mdf-2(tm2190)* allele was received from Dr. A. Golden. **Some strains were provided by the CGC, which is funded by NIH Office of Research Infrastructure Programs (P40 OD010440).**

Strain #	Genotype
UM399	*ltIs37[unc-119(+), Ppie-1::mCherry::HIS-58] IV; ojIs1[unc-119(+), Ppie-1::GFP::tbb-2] V*
UM471	*zyg-1(or297) II; ltIs37[unc-119(+), Ppie-1::mCherry::HIS-58] IV; ojIs1[unc-119(+), Ppie-1::GFP::tbb-2] V*
UM547	*tbb-2(or362) III; ltIs37[unc-119(+), Ppie-1::mCherry::HIS-58] IV; ddIs6 [tbg-1::GFP, unc-119(+)] V*
UM525	*zyg-1(or297) II; mdf-2(tm2190), ltIs37[unc-119(+), Ppie-1::mCherry::HIS-58] IV; ojIs1[unc-119(+), Ppie-1::GFP::tbb-2] V*
UM548	*zyg-1(or297) II; ltIs37[unc-119(+), Ppie-1::mCherry::HIS-58] IV*
UM572	*zyg-1(or297) II; unc-45(e286), par-2(lw32)/qC1[dpy-19(e1259), glp-1(q339)] III; ltIs37[unc-119(+), Ppie-1::mCherry::HIS-58] IV; ojIs1[unc-119(+), Ppie-1::GFP::tbb-2] V*
UM573	*zyg-1(or297) II; ltIs37[unc-119(+), Ppie-1::mCherry::HIS-58] IV; sqt-3(sc8), par-1(it51) V/nT1[unc-?(n754) let-?] (IV;V)*
UM628	*zyg-1(or297) II; unc-45(e286) III; ltIs37[unc-119(+), Ppie-1::mCherry::HIS-58] IV; ojIs1[unc-119(+), Ppie-1::GFP::tbb-2] V*
UM627	*zyg-1(or297) II; ltIs37[unc-119(+), Ppie-1::mCherry::HIS-58] IV; sqt-3(sc8) V*
UM463	*cpIs42[mex-5p::mNeonGreen::PLCδ-PH::tbb-2 3'UTR, unc-119(+)] II; ltIs37[unc-119(+), Ppie-1::mCherry::HIS-58] IV*

UM664	*zyg-1(or297) II; lon-1(e185), par-3(it71)/qC1 [dpy-19(e1259) glp-1(q339)] III; ltIs37[unc-119(+), Ppie-1::mCherry::HIS-58] IV; ojIs1[unc-119(+), Ppie-1::GFP::tbb-2] V*
UM665	*zyg-1(or297) II; lon-1(e185) III; ltIs37[unc-119(+), Ppie-1::mCherry::HIS-58] IV; ojIs1[unc-119(+), Ppie-1::GFP::tbb-2] V*

Table S2. Summary statistics. Related to all figures. Summary statistics are provided for all data included in the manuscript text and figures. Data are listed by order of figure. See Materials and Methods for details on data normalization and statistical analyses. $\bar{x}$ = sample mean. CI = confidence interval. SD = standard deviation. μ = population mean. σ = population standard deviation. m = slope. b = intercept. r = Pearson's coefficient. See Experimental Procedures for details.

Video Legends

Videos 1, 2 and 5 were acquired on a Cell Observer SD spinning disc confocal (Zeiss; Yokogawa) equipped with a stage-top incubator (Pecon) set to 26ºC, using an AxioCam 506 Mono camera (Zeiss), with 4x4 binning, and a 63x/1.4 NA Plan Apochromat DIC oil immersion objective (Zeiss) in Zen software (Zeiss). Images were acquired every 30 seconds, with the exception of Video 4 (*mdf-1*(RNAi)) which was acquired every 33 seconds. Images were processed using ImageJ (NIH). Maximum intensity projections of 18 z-slices (1µm sectioning) centered on the embryo of interest are shown. All embryos are oriented with anterior to the left. Scale bar = 10µm. Videos 3 and 4 were acquired on a Cell Observer SD spinning disc confocal (Zeiss; Yokogawa) at room temperature (~20ºC), using an AxioCam 506 Mono camera (Zeiss), with 3x3 binning, and a 40x/1.4 NA Plan Apochromat DIC (UV) VIS-IR oil immersion objective (Zeiss), in Zen software (Zeiss). Images were acquired every 30.3 seconds for Video 3 and every 45.4 seconds for Video 4. Maximum intensity projections of 5 z-slices (1.5µm sectioning) centered on the nucleus of interest are shown. Scale bar = 5µm. For all Videos, images were adjusted for brightness and contrast and scaled 4 times to adjust for file compression during .avi conversion. For all Videos except 2, H2B::mCH is shown in cyan and β-tubulin::GFP is shown in red. For Video 2, H2B::mCH is shown in cyan and γ-tubulin::GFP is shown in red. Time stamp is in min:sec. Videos play at 4 frames per second.

Video S1. zyg-1(ts)-induced monopolar spindles in 2- and 4-cell stage embryos.

Video S2. tbb-2(ts)-induced spindle defects in 2- and 4-cell stage embryos.

Video S3. A P_2 cell from a permeabilized embryo treated with DMSO.

Video S4. A P_2 cell from a permeabilized embryo treated with 33µM Nocodazole.

Video S5. zyg-1(ts)-induced monopolar spindles in 2- and 4-cell stage embryos following RNAi depletion of MDF-1.